
Extraction of hierarchical functional connectivity components in human brain using resting-state fMRI

Dushyant Sahoo

University of Pennsylvania
sadu@seas.upenn.edu

Danielle Bassett
University of Pennsylvania

Christos Davatzikos
University of Pennsylvania

Abstract

The study of hierarchy in networks of the human brain has been of significant interest among the researchers as numerous studies have pointed out towards a functional hierarchical organization of the human brain. This paper provides a novel method for the extraction of hierarchical connectivity components in the human brain using resting-state fMRI. The method builds upon prior work of Sparse Connectivity Patterns (SCPs) by introducing a hierarchy of sparse overlapping patterns. The components are estimated by deep factorization of correlation matrices generated from fMRI. The goal of the paper is to extract interpretable hierarchical patterns using correlation matrices where a low rank decomposition is formed by a linear combination of a high rank decomposition. We formulate the decomposition as a non-convex optimization problem and solve it using gradient descent algorithms with adaptive step size. We also provide a method for the warm start of the gradient descent using singular value decomposition. We demonstrate the effectiveness of the developed method on two different real-world datasets by showing that multi-scale hierarchical SCPs are reproducible between sub-samples and are more reproducible as compared to single scale patterns. We also compare our method with existing hierarchical community detection approaches. Our method also provides novel insight into the functional organization of the human brain.

1 Introduction

It has been known that the human brain consists of spatially different regions which are functionally connected to form networks^[22]. In addition, these networks are claimed to be hierarchically organized in the brain^[6;17;10;16]. However, our understanding of the hierarchical nature of these networks is limited which might be attributed to their complex nature. Most of the existing methods such as Independent Component Analysis (ICA)^[2], Sparse Dictionary Learning (DL)^[8] and graph theory based network analysis^[3] for analysis of functional networks are focused on estimating a fixed number of networks with no hierarchy. If the assumption about the hierarchy is true then the original data might contain complex hierarchical information with implicit lower-level hidden attributes, that classical one level connectivity methodologies would not be able to capture effectively and interpretably.

Most of the methods used for estimation of hierarchical networks in fMRI data analysis are of agglomerative (“bottom-up”) type such as Hierarchical clustering^[25;15], Hierarchical Community Detection^[1] where the method begins by regarding each element as a separate network and then merging them into larger networks successively. Most of the hierarchical community detection

approaches assume that the communities are independent, but this is not the case in the human brain where it is known the certain brain regions interact with multiple networks i.e. the networks overlap. But only a few hierarchical community detection methods^[13;21;26] have been developed which find overlapping communities. However, the community detection approaches are not equipped to handle connectivity analysis of fMRI data. This is because the negative edge links are treated as repulsion whereas in resting fMRI, a negative edge link has same information but with opposing phase^[19]. Assigning anti-correlated and correlated regions to the same network can reveal much more information about the functional organization of the human brain network^[9]. Recently,^[14] used Deep Semi Non Negative Matrix Factorization^[23] for estimating hierarchical overlapping functional networks. The model given by^[14] could only find networks containing regions with positive correlation between them as the method is based on non-negative matrix factorization thus limiting the model to only use positive matrices.

Our work fills the above gap by modeling the fMRI data to capture essential properties of the network, namely- 1) Sparsity: only some nodes interact with other nodes in a given network, 2) Heterogeneity: some networks might be more prominent in particular individuals as compared to others, 3) Existence of positively and negatively correlated nodes in a network 4) Overlapping networks, which is likely to reflect true brain organization, as brain networks might share certain regional components and 5) Hierarchy: By adding extra layers of abstraction we can learn latent attributes and the hierarchy in the networks. Our method is built upon Sparse Connectivity Patterns (SCPs)^[9] with the aim of finding Hierarchical Sparse Connectivity Patterns (HSCPs) which are estimated by jointly decomposing correlation matrices into multiple decomposition having different ranks using a deep framework for matrix factorization. Extraction of HSCPs helps in mitigating the noise in individual scans by jointly decomposing the correlation matrices obtained from the subject of a population into a common set of hierarchical sparse low-rank components . We use gradient descent with adaptive step size for solving non-convex optimization and have also introduced an initialization algorithm for faster convergence. We evaluate the representation learned by the model on two different real datasets and compare it with EAGLE^[21] which is a well known hierarchical overlapping community detection algorithm.

The organization of the remainder of the paper as follows. In Section 2 we present the method for the extraction of HSCPs shared between rs-fMRI scans. Section 3 presents experimental results for validation of the method on the rs-fMRI scans of the 100 unrelated HCP subjects and 969 subjects from PNC data set. We conclude with discussion.

2 Method

2.1 SCP

Let $\mathbf{X}^i \in \mathbb{R}^{P \times T}$ be the fMRI data of the i^{th} subject having P regions and T time points, and $\Sigma^i \in \mathbb{S}_{++}^{P \times P}$ is the correlation matrix where $\Sigma_{m,o}^i = \text{corr}(\mathbf{x}_m^i, \mathbf{x}_o^i)$ is the correlation between time series of m^{th} and o^{th} node. We first define the model for estimating the Sparse Connectivity Patterns (SCPs)^[9] in the fMRI data which decomposes the correlation matrices into non-negative linear combination of sparse low rank components such that for all $i = 1, \dots, S$ we have $\Sigma^i = \mathbf{W}\Lambda^i\mathbf{W}^T$ where $\mathbf{W} \in \mathbb{R}^{P \times k}$ is a set of shared patterns across all subjects, $k < P$ and $\Lambda^i \succeq 0$ is a diagonal matrix storing the subject specific information about the contribution of each of the components. Let $\mathbf{w}_l \in \mathbb{R}^P$ be the l^{th} column of \mathbf{W} such that $-1 \preceq \mathbf{w}_l \preceq 1$ and let $w_{l,s}$ be the s^{th} element of \mathbf{w}_l vector, then \mathbf{w}_l represents a component which reflects the weights of the nodes in the component and if $w_{l,s}$ is zero then s^{th} node does not belong to l^{th} component. If the sign of weights of any two nodes in a component is same then they are positively correlated else they have anti-correlation. To make the patterns sparse, each column of \mathbf{W} was subjected to L_1 penalty and the below optimization is solved to obtain the SCPs

$$\begin{aligned} & \underset{\mathbf{W}, \Lambda}{\text{minimize}} && \sum_{i=1}^S \|\Sigma^i - \mathbf{W}\Lambda^i\mathbf{W}^T\|_F^2 \\ & \text{subject to} && \|\mathbf{w}_l\|_1 \leq \lambda, l = 1, \dots, k \\ & && \|\mathbf{w}_l\|_\infty \leq 1, l = 1, \dots, k \\ & && \Lambda^i \succeq 0, i = 1, \dots, S \end{aligned} \tag{1}$$

where S is the total number of subjects and λ controls the sparsity of the components.

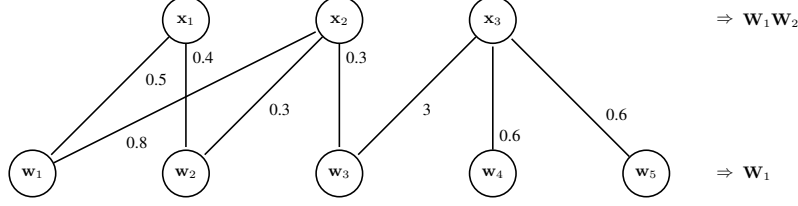


Figure 1: Example of 2-layer hierarchical structure

2.2 HSCP

We have extended the above work and introduced Hierarchical Sparse Connectivity Patterns (HSCPs) to estimate hierarchical sparse low rank patterns in the correlation matrices. In our model, a correlation matrix is decomposed into K levels as -

$$\Sigma^i \approx \mathbf{W}_1 \Lambda_1^i \mathbf{W}_1^T \approx \mathbf{W}_1 \mathbf{W}_2 \Lambda_2^i \mathbf{W}_2^T \mathbf{W}_1^T \approx \dots \approx \mathbf{W}_1 \mathbf{W}_2 \dots \mathbf{W}_K \Lambda_K^i \mathbf{W}_K^T \mathbf{W}_K^T \mathbf{W}_{K-1}^T \dots \mathbf{W}_1^T \quad (2)$$

where $\mathbf{W}_1 \in \mathbb{R}^{P \times k_1}$ and $\mathbf{W}_q \in \mathbb{R}^{k_{q-1} \times k_q}$, $\Lambda_q^i \in \mathbb{R}^{k_q \times k_q}$ is a diagonal matrix storing subject specific information of the patterns and $n > k_1 > k_2 > \dots > k_K$ and \mathbf{W}^T is the transpose of \mathbf{W} . Here k_r is the number of components at the r^{th} level, note that k_1 is the number of components at the lower most level of the hierarchy.

For better interpretability and noise reduction in the model, we have introduced sparsity constraints on the \mathbf{W} matrices. By making \mathbf{W}_1 sparse we are forcing the components to contain few number of nodes and by forcing rest of the \mathbf{W} s to be sparse, we are forcing that the components at each of the next level are sparse linear combination of previous components. If we consider 2 layer hierarchical representation of a given correlation matrix then we can define $\mathbf{Z}_1 = \mathbf{W}_1 \mathbf{W}_2$ to be a $P \times k_2$ matrix, then \mathbf{Z}_1 is a coarse network which consist of weighted linear combination of \mathbf{W}_1 which are fine level components where weights are stored in \mathbf{W}_2 . Fig.1 is an example of 2 layer hierarchical structure where \mathbf{w} s are columns of \mathbf{W}_1 and \mathbf{x} s are columns of $\mathbf{W}_1 \mathbf{W}_2$, and $k_1 = 5$ and $k_2 = 3$. Let $\mathcal{W} = \{\mathbf{W}_1, \dots, \mathbf{W}_K\}$ and $\mathcal{L} = \{\Lambda_1, \dots, \Lambda_K\}$ The hierarchical networks can be estimated by solving the below minimization problem

$$\begin{aligned} \underset{\mathcal{W}, \mathcal{L}}{\text{minimize}} \quad & H(\mathcal{W}, \mathcal{L}) = \sum_{i=1}^S \sum_{r=1}^K \|\Sigma^i - (\Pi_{j=1}^r \mathbf{W}_j) \Lambda_r^i (\Pi_{n=1}^r \mathbf{W}_n)^T\|_F^2 \\ \text{subject to} \quad & \|\mathbf{w}_l^r\|_1 < \lambda_r, l = 1, \dots, k_r \quad \text{and} \quad r = 1, \dots, K \\ & \|\mathbf{w}_l^r\|_\infty \leq 1, l = 1, \dots, k_r \quad \text{and} \quad r = 1, \dots, K \\ & \mathbf{W}_j \geq 0, j = 2, \dots, K \\ & \Lambda_r^n \succeq 0, i = 1, \dots, S \quad \text{and} \quad r = 1, \dots, K \end{aligned} \quad (3)$$

The optimization problem defined in 3 is a non-convex problem which we solved using alternating minimization. Below are the gradients of H with respect to \mathcal{W} and \mathcal{L} . Let us first define the following variables

$$\begin{aligned} \mathbf{W}_0 &= \mathbf{I}_P \\ \mathbf{Y}_r &= \Pi_{j=0}^r \mathbf{W}_j \\ \mathbf{T}_{n,i}^r &= \Pi_{j=0}^{n-r} \mathbf{W}_j \Lambda_j^n (\Pi_{j=0}^{n-r} \mathbf{W}_j)^T \end{aligned}$$

the gradient of H with respect to Λ_r^i is:

$$\frac{\partial H}{\partial \Lambda_r^i} = (-2 \mathbf{Y}_r^T \Sigma_r^i \mathbf{Y}_r + 2 \mathbf{Y}_r^T \mathbf{Y}_r \Lambda_r^T \mathbf{Y}_r) \circ \mathbf{I}_{k_r}$$

the gradient of H with respect to \mathbf{W}_l is written as:

$$\frac{\partial H}{\partial \mathbf{W}_r} = \sum_{i=1}^S \sum_{j=r}^K 4 \mathbf{Y}_{r-1}^T \mathbf{Y}_{r-1} \mathbf{W}_r \mathbf{T}_j^r \mathbf{W}_r^T \mathbf{Y}_{r-1}^T \mathbf{Y}_{r-1} \mathbf{W}_r \mathbf{T}_j^r - 4 \mathbf{Y}_{r-1}^T \Sigma_i \mathbf{Y}_{r-1} \mathbf{W}_r \mathbf{T}_j^k$$

Algorithm 1 Initialization

```

1: Input: Data  $\Sigma$ 
2: for  $i = 1$  to  $S$  do
3:   for  $r = 1$  to  $K$  do
4:     if  $r == 1$  then
5:        $\mathbf{U}^i \mathbf{V}^i (\mathbf{U}^i)^T = \text{SVD}(\Sigma^i)$ 
6:     else
7:        $\mathbf{U} \mathbf{V} \mathbf{U}^T = \text{SVD}(\Lambda_{r-1}^i)$ 
8:      $\Lambda_k^i = \mathbf{V}^i$ 
9:      $\mathbf{W}_r = \frac{1}{S} \sum_{i=1}^S (\mathbf{U}^i)$ 
10: Output:  $\mathcal{W}$  and  $\mathcal{L}$ 

```

Algorithm 2 SHCP

```

1: Input: Data  $\Sigma$ , number of connectivity patterns
    $k_1, \dots, k_K$  and sparsity  $\lambda_1, \dots, \lambda_K$  at different level
2:  $\mathcal{W}$  and  $\mathcal{L} = \text{Initialization}(\Sigma)$ 
3: repeat
4:   for  $r = 1$  to  $K$  do
5:      $\mathbf{W}_r \leftarrow \text{descent}(\mathbf{W}_r)$ 
6:      $\mathbf{W}_r \leftarrow \text{proj}_1(\mathbf{W}_r, \lambda_r)$ 
7:     if  $r > 1$  then
8:        $\mathbf{W}_r \leftarrow \text{proj}_2(\mathbf{W}_r)$ 
9:     for  $i = 1, \dots, S$  do
10:       $\Lambda_r^i \leftarrow \text{descent}(\Lambda_r^i)$ 
11:       $\Lambda_r^i \leftarrow \text{proj}_2(\Lambda_r^i)$ 
12: until Stopping criterion is reached
13: Output:  $\mathcal{W}$  and  $\mathcal{L}$ 

```

Algorithm 2 describes the complete alternating minimization procedure where $\text{proj}_1(\mathbf{W}, \lambda)$ operator projects each column of \mathbf{W} into intersection of L_1 and L_∞ ball, and proj_2 projects a matrix onto \mathbb{R}_+ by making all the negative elements in the matrix equal to zero. As the gradients are not globally Lipschitz, we don't have bounds on the step size for the gradients. For that reason, we have used AMSGrad^[18], ADAM^[12] and NADAM^[7] as gradient descent algorithms which have adaptive step size. descent is the update rule used by different gradient descent techniques. All the code is implemented in MATLAB and will be released upon publication.

In the above formulation, the last level has the highest number of components k_1 , and in the level after that we have k_2 number of components which are linear combination of components at previous level, so on and so forth. In this way, we have built up a hierarchical model where each component is made up of linear combination of components at the previous hierarchy. Note that we can not just use the last decomposition in the above architecture to get the hierarchy as different layers have different ranks and different approximations, hence we will need all the approximations to build the hierarchical structure. In addition, one would expect \mathbf{W}_2 and \mathbf{W}_s to be degenerate, but that would be the case only when \mathbf{W}_1 is orthogonal matrix. Consider the case where we have a two level hierarchy, we can have better approximation by taking a linear combination of columns of \mathbf{W}_1 which we have also observed empirically.

2.3 Initialization

SHCP decomposition at single level is very similar to Singular Value Decomposition (SVD) but with the dependent components. Hence, we believe that the final components we estimate are a modification of singular vectors. Thus, we have initialized the \mathcal{W} and \mathcal{L} by taking SVD of input data matrix which also makes our algorithm deterministic. Algorithm 1 describes the initialization algorithm. We empirically show in the next section that SVD initialization results in faster convergence.

3 Experiments

3.1 Dataset

We used two real dataset for validation of the method which are described below

- HCP- Human Connectome Project (HCP)^[24] dataset is one of the widely used dataset for fMRI analysis containing fMRI scans of 100 unrelated subjects which were processed using ICA+FIX pipeline with MSMAll registration^[11]. Each subject has 4004 time points and the time series were normalized to zero mean and unit L2 norm, averaged over the 360 nodes of the multimodal HCP parcellation^[11], and the average time series were normalized to zero mean and unit L2 norm.
- PNC- Philadelphia Neuro-developmental Cohort (PNC)^[20] dataset contains 969 subjects each having 120 time points and 121 nodes. The data were preprocessed using an optimized procedure^[4] which includes slice timing, confound regression, and band-pass filtering.

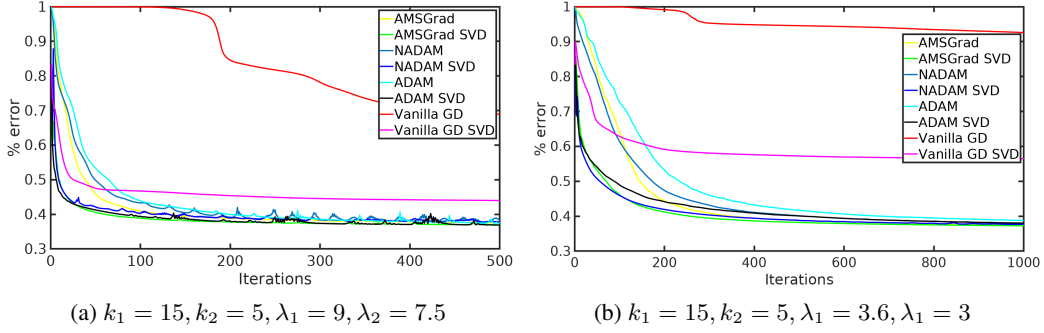


Figure 2: Performance comparison of different gradient descent techniques. here is defined asD corresponds to gradient descent with SVD initialization

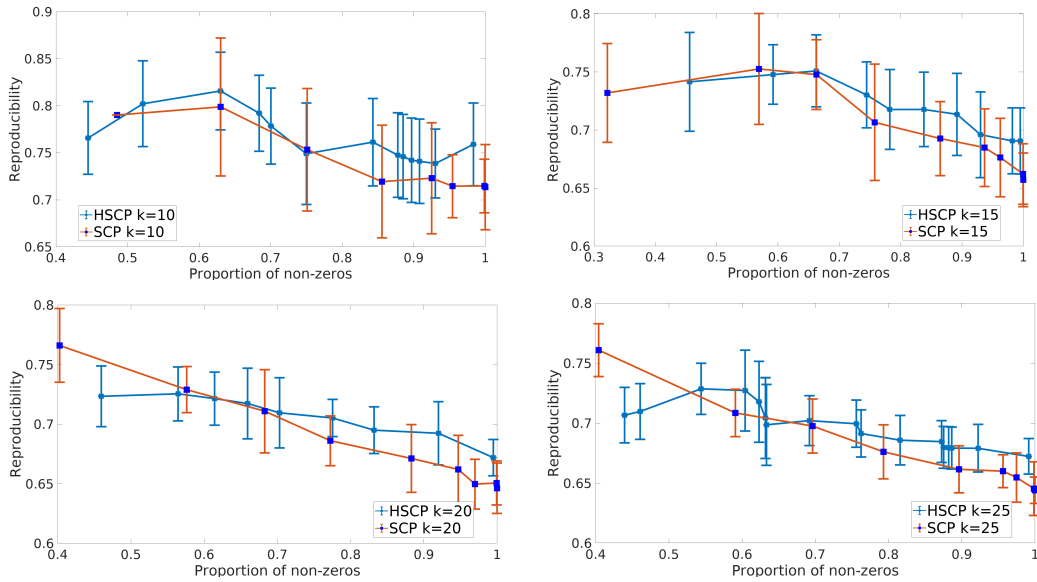


Figure 3: Comparison of single scale (SCP) and hierarchical (HSCP) components on HCP dataset.

3.2 Convergence Analysis

We compare AMSGrad, ADAM, NADAM and vanilla gradient descent with SVD initialization and random initialization by measuring percentage error which is defined as:

$$\frac{\sum_{i=1}^S \sum_{r=1}^K \|\Sigma^i - (\Pi_{j=1}^r \mathbf{W}_j) \Lambda_r^i (\Pi_{n=1}^r \mathbf{W}_n)^T\|_F^2}{\sum_{i=1}^S \sum_{r=1}^K \|\Sigma^i\|_F^2}$$

For fair comparison, we set $\beta_1 = 0.9$ and $\beta_2 = 0.99$ for ADAM, NADAM and AMSGRAD algorithm. Figure 2 shows the convergence of the algorithm on the complete HCP data for two different combinations of sparsity parameters at a particular set of k_1 and k_2 . From the Figure 2 we can see that the AMSGrad has the best convergence. For rest of the experiments we have used AMSGrad algorithm to perform gradient descent.

3.3 Comparison with single scale components

For validating the hierarchical model, we compared the reproducibility of components extracted from hierarchical model (HSCP) versus single scale components (SCP). Reproducibility here is defined as the normalized inner product of components derived from the two equal random sub-samples of the data averaged across all the components. We compare components derived from HSCP with $k_1 \in \{10, 15, 20, 25\}$, $k_2 \in \{4, 5, 6, 8\}$, $\lambda_1 \in P \times 5(10^{[-3:-1]})$ and $\lambda_2 \in k_1 \times 10^{[-3:-1]}$, and from

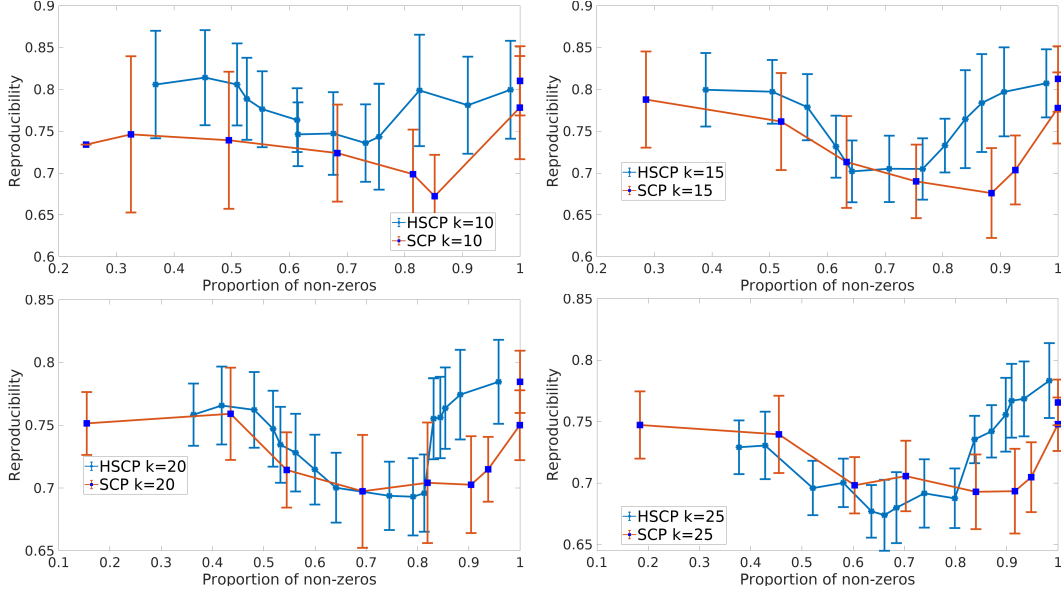


Figure 4: Comparison of single scale (SCP) and hierarchical (HSCP) components on PNC dataset.

		10	15	20	25
4	HSCP	0.8885±0.0441	0.8351±0.0748	0.8507±0.0635	0.8567±0.0615
	EAGLE	0.3077±0.098	0.4158±0.1321	-	-
5	HSCP	0.8753±0.0348	0.8356±0.0591	0.8281±0.0656	0.8161±0.0531
	EAGLE	0.2908±0.0737	0.2664±0.0333	0.0792±0.1656	0.5033±0.1756
6	HSCP	0.8756±0.0375	0.8461±0.0486	0.8224±0.0555	0.8215±0.0447
	EAGLE	0.2356±0.0196	0.3209±0.1206	0.3717±0.1698	0.3885±0.1395
8	HSCP	0.8781±0.0694	0.8389±0.0479	0.8240±0.046	0.8267±0.0548
	EAGLE	-	-	0.3374±0.167	0.4682±0.2349

Table 1: Reproducibility Comparison (mean±std) on HCP dataset. The rows correspond to values of k_1 and the columns correspond to values of k_2 .

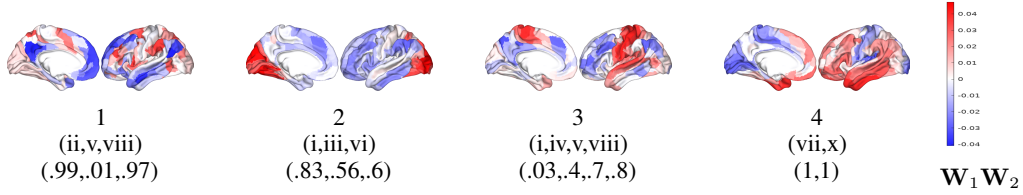
SCP with $k \in \{4, 5, 6, 8, 10, 15, 20, 25\}$ at $\lambda \in P \times 5(10^{[-4:-1]})$. At a fixed k_2 and λ_2 , we find the optimal k_1 and λ_1 by dividing the data into 3 equal parts: training, validation and test data, and choosing the parameters corresponding to maximum reproducibility over 20 runs on training and validation set. Figure 3 and Figure 4 show the reproducibility of the components averaged over 20 runs on training and test data. We can see that the same number of components extracted from second level using HSCP are on an average more reproducible than the components extracted using SCP.

3.4 Comparison with EAGLE

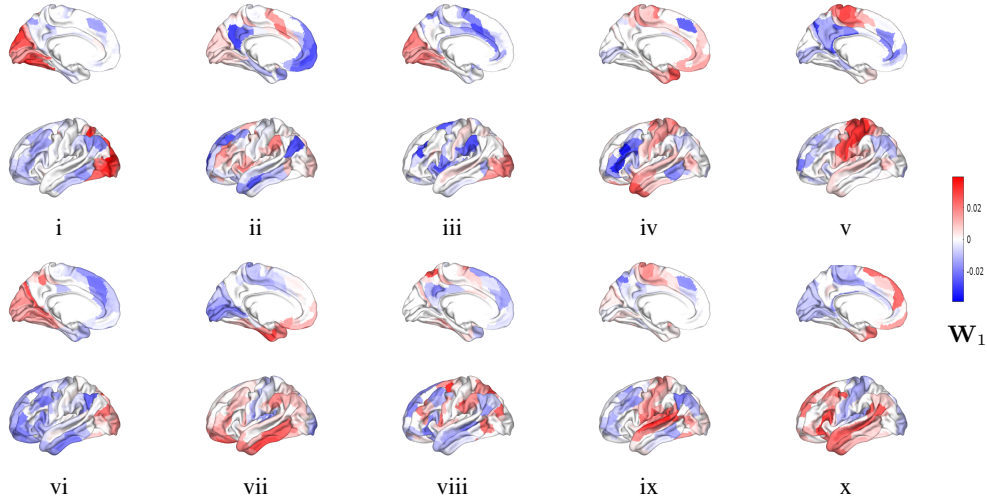
We compared the reproducibility of hierarchical components extracted from HSCP to hierarchical overlapping communities obtained using EAGLE^[21]. Implementation of EAGLE was obtained from the authors. Correlation matrix averaged across all the subjects was used as an input to EAGLE. Hierarchical components and communities with $k_1 \in \{10, 15, 20, 25\}$, $k_2 \in \{4, 5, 6, 8\}$ were generated from HSCP and EAGLE. Optimal λ_1 and λ_2 for HSCP were selected by dividing the data into three equal parts: training, validation and test set, and performing the validation procedure as described in section 3.3. Reproducibility was computed using training and test for both HSCP and EAGLE for all combinations of k_1 and k_2 . Table1 and Table2 show the reproducibility results on HCP and PNC datasets. For a particular k_1 and k_2 , reproducibility table show the average of the two reproducibility values. Some cells in the tables are empty as the EAGLE algorithm was not able to

		10	15	20	25
4	HSCP	0.8838±0.0495	0.7998±0.0766	0.8036±0.0599	0.7726±0.059
	EAGLE	.6287±0.3005	0.6433±0.1321	-	-
5	HSCP	0.8785±0.0675	0.8379±0.0704	0.8099±0.0736	0.8062±0.0459
	EAGLE	0.6575±0.1973	0.5327±0.1828	0.5426±0.1656	0.7229±0.1349
6	HSCP	0.8655±0.0404	0.8364±0.649	0.8518 ±0.0587	0.7912±0.0433
	EAGLE	0.7571±0.2366	0.6279±0.1011	0.6244±0.2627	0.7361±0.2449
8	HSCP	0.867 ±0.0559	0.8347± 0.0517	0.8340±0.0657	0.8058 ±0.0447
	EAGLE	0.7997±0.0323	0.7451±0.0319	0.5933±0.2126	0.7183±0.0708

Table 2: Reproducibility Comparison (mean±std) on PNC dataset. The rows correspond to values of k_1 and the columns correspond to values of k_2 .



(a) 4 coarse scale components ($\mathbf{W}_1\mathbf{W}_2$). Below each component number is the information about the fine level components and their weights used to compute the coarse components.



(b) 10 fine scale components (\mathbf{W}_1). ii and viii show different regions of Default Mode anti-correlated with the Salience and Cingulo-Opercular system. v show different regions of default mode anti-correlated with the sensori-motor areas. iii and vi shows different regions of Visual system anti-correlated with Salience and Default Mode.

Figure 5: Hierarchical components derived from HCP dataset. Nodes with red and blue color are correlated among themselves, but are anticorrelated with each other.

generate hierarchical structures for particular values of k_1 and k_2 . The results clearly show that the HSCPs have better reproducibility than the communities derived using EAGLE.

3.5 Results from resting state fMRI

From the complete HCP dataset, we extracted the 4 coarse components ($\mathbf{W}_1\mathbf{W}_2$) and 10 fine components (\mathbf{W}_1) that exhibited the highest reproducibility between the training and test sets. Figure 5b displays the 10 fine level components and Figure 5a displays the 4 coarse level components. It can be clearly seen from Figure5 that the fine and coarse level components are overlapping and sparse,

and coarse components are comprised of sparse linear combination of fine level components which helps in discovering the relation between different networks at different scales.

The 10 fine level components obtained show the relation between different functional networks and are similar to the SCPs extracted in^[9]. The 4 coarse level components obtained are the brain states defined by^[5]. Component 1 is similar to DMN+, component 2 is similar to VIS+, component 3 is similar to FNM+, component 4 is similar to DMN- where^[5] describes DMN+, VIS+, FNM+ and DMN- as brain states which have overlapping regions. As per the convention of^[5], DMN+ represents high activity in Default Mode Network and low activity in Dorsal Attention Network, DMN- represents with high activity in Visual Network and low activity in Default Mode Network, VIS+ represents with high activity in Visual Network and low activity in Ventral Attention Network and FNM+ represents with high activity in Frontal Network and low activity in Somatomotor Network. Another important observation to notice is that each of the coarse component comprises of fine level components having major functional networks and their relation with other nodes. For instance, coarse component 1 comprises majorly of ii and viii which stores the relation between regions of Default Mode network and other nodes in the brain. Similarly, coarse component 2 stores the relation between visual regions and rest of the regions in the brain using i, iii and vi. Thus, HSCPs can provide novel insights into functioning of brain by jointly uncovering both fine and coarse level components with the coarse components comprised of similarly functioning fine components.

4 Conclusions

In this work, we proposed a novel technique for extraction of hierarchical sparse components from correlation matrices corresponding to each subject as an independent observation. We formulated the problem as non-convex optimization and used adaptive learning rate based gradient descent algorithm to solve it. Our method is able to find sparse, low rank hierarchical decomposition using deep matrix matrix factorization which is highly reproducible across data-sets. Our model computationally extracts a set of hierarchical components common across subjects, including resting state networks. At the same time, we capture individual information about subjects as a linear combination of these hierarchical components, making it a useful measure for group studies. Importantly, our work provides a method to uncover hierarchical organization in the functioning of the human brain. Results of our method can provide novel insights towards uncovering crucial properties of the human brain function.

References

- [1] Arian Ashourvan, Qawi K Telesford, Timothy Verstynen, Jean M Vettel, and Danielle S Bassett. Multi-scale detection of hierarchical community architecture in structural and functional brain networks. *arXiv preprint arXiv:1704.05826*, 2017.
- [2] Christian F Beckmann, Marilena DeLuca, Joseph T Devlin, and Stephen M Smith. Investigations into resting-state connectivity using independent component analysis. *Philosophical Transactions of the Royal Society B: Biological Sciences*, 360(1457):1001–1013, 2005.
- [3] Ed Bullmore and Olaf Sporns. Complex brain networks: graph theoretical analysis of structural and functional systems. *Nature reviews neuroscience*, 10(3):186, 2009.
- [4] Rastko Ciric, Daniel H Wolf, Jonathan D Power, David R Roalf, Graham L Baum, Kosha Ruparel, Russell T Shinohara, Mark A Elliott, Simon B Eickhoff, Christos Davatzikos, et al. Benchmarking of participant-level confound regression strategies for the control of motion artifact in studies of functional connectivity. *Neuroimage*, 154:174–187, 2017.
- [5] Eli J Cornblath, Arian Ashourvan, Jason Z Kim, Richard F Betzel, Rastko Ciric, Graham L Baum, Xiaosong He, Kosha Ruparel, Tyler M Moore, Ruben C Gur, et al. Context-dependent architecture of brain state dynamics is explained by white matter connectivity and theories of network control. *arXiv preprint arXiv:1809.02849*, 2018.
- [6] Gaëlle Doucet, Mikaël Naveau, Laurent Petit, Nicolas Delcroix, Laure Zago, Fabrice Crivello, Gael Jobard, Nathalie Tzourio-Mazoyer, Bernard Mazoyer, Emmanuel Mellet, et al. Brain activity at rest: a multiscale hierarchical functional organization. *Journal of neurophysiology*, 105(6):2753–2763, 2011.

- [7] Timothy Dozat. Incorporating nesterov momentum into adam. 2016.
- [8] Harini Eavani, Roman Filipovych, Christos Davatzikos, Theodore D Satterthwaite, Raquel E Gur, and Ruben C Gur. Sparse dictionary learning of resting state fmri networks. In *2012 Second International Workshop on Pattern Recognition in NeuroImaging*, pages 73–76. IEEE, 2012.
- [9] Harini Eavani, Theodore D Satterthwaite, Roman Filipovych, Raquel E Gur, Ruben C Gur, and Christos Davatzikos. Identifying sparse connectivity patterns in the brain using resting-state fmri. *Neuroimage*, 105:286–299, 2015.
- [10] Luca Ferrarini, Ilya M Veer, Evelinda Baerends, Marie-José van Tol, Remco J Renken, Nic JA van der Wee, Dirk J Veltman, Andre Aleman, Frans G Zitman, Brenda WJH Penninx, et al. Hierarchical functional modularity in the resting-state human brain. *Human brain mapping*, 30(7):2220–2231, 2009.
- [11] Matthew F Glasser, Stamatios N Sotiropoulos, J Anthony Wilson, Timothy S Coalson, Bruce Fischl, Jesper L Andersson, Junqian Xu, Saad Jbabdi, Matthew Webster, Jonathan R Polimeni, et al. The minimal preprocessing pipelines for the human connectome project. *Neuroimage*, 80:105–124, 2013.
- [12] Diederik P Kingma and Jimmy Ba. Adam: A method for stochastic optimization. *arXiv preprint arXiv:1412.6980*, 2014.
- [13] Andrea Lancichinetti, Santo Fortunato, and Janos Kertesz. Detecting the overlapping and hierarchical community structure in complex networks. *New Journal of Physics*, 11(3):033015, 2009.
- [14] Hongming Li, Xiaofeng Zhu, and Yong Fan. Identification of multi-scale hierarchical brain functional networks using deep matrix factorization. In *International Conference on Medical Image Computing and Computer-Assisted Intervention*, pages 223–231. Springer, 2018.
- [15] Xiao Liu, Xiao-Hong Zhu, Peihua Qiu, and Wei Chen. A correlation-matrix-based hierarchical clustering method for functional connectivity analysis. *Journal of neuroscience methods*, 211(1):94–102, 2012.
- [16] David Meunier, Renaud Lambiotte, Alex Fornito, Karen Ersche, and Edward T Bullmore. Hierarchical modularity in human brain functional networks. *Frontiers in neuroinformatics*, 3:37, 2009.
- [17] Hae-Jeong Park and Karl Friston. Structural and functional brain networks: from connections to cognition. *Science*, 342(6158):1238411, 2013.
- [18] Sashank J Reddi, Satyen Kale, and Sanjiv Kumar. On the convergence of adam and beyond. 2018.
- [19] Mikail Rubinov and Olaf Sporns. Weight-conserving characterization of complex functional brain networks. *Neuroimage*, 56(4):2068–2079, 2011.
- [20] Theodore D Satterthwaite, Mark A Elliott, Kosha Ruparel, James Loughhead, Karthik Prabhakaran, Monica E Calkins, Ryan Hopson, Chad Jackson, Jack Keefe, Marisa Riley, et al. Neuroimaging of the philadelphia neurodevelopmental cohort. *Neuroimage*, 86:544–553, 2014.
- [21] Huawei Shen, Xueqi Cheng, Kai Cai, and Mao-Bin Hu. Detect overlapping and hierarchical community structure in networks. *Physica A: Statistical Mechanics and its Applications*, 388(8):1706–1712, 2009.
- [22] Olaf Sporns. *Networks of the Brain*. MIT press, 2010.
- [23] George Trigeorgis, Konstantinos Bousmalis, Stefanos Zafeiriou, and Björn W Schuller. A deep matrix factorization method for learning attribute representations. *IEEE transactions on pattern analysis and machine intelligence*, 39(3):417–429, 2017.

- [24] David C Van Essen, Stephen M Smith, Deanna M Barch, Timothy EJ Behrens, Essa Yacoub, Kamil Ugurbil, Wu-Minn HCP Consortium, et al. The wu-minn human connectome project: an overview. *Neuroimage*, 80:62–79, 2013.
- [25] Yanlu Wang and Tie-Qiang Li. Analysis of whole-brain resting-state fmri data using hierarchical clustering approach. *PloS one*, 8(10):e76315, 2013.
- [26] Zhiwei Zhang and Zhenyu Wang. Mining overlapping and hierarchical communities in complex networks. *Physica A: Statistical Mechanics and its Applications*, 421:25–33, 2015.